Targeting heparan sulfate proteoglycan-assisted endocytosis as a COVID-19 therapeutic option

Qi Zhang[1], Catherine Z. Chen[2], Manju Swaroop[2], Miao Xu[2], Lihui Wang[1], Juhyung Lee[1], Manisha Pradhan[2], Min Shen[2], Zhiji Luo[2], Yue Xu[1], Wenwei Huang[2], Wei Zheng[2], Yihong Ye[1]

[1] Laboratory of Molecular Biology, National Institute of Diabetes and Digestive and Kidney Diseases, National Institutes of Health, Bethesda, MD 20892

[2] National Center for Advancing Translational Sciences, National Institutes of Health, Rockville, MD 20850

Correspondence should be sent to:

Yihong Ye

email: yihongy@mail.nih.gov

Tel: 301-594-0845

Fax: 301-496-0201

Running title: HSPG assists ACE2 in coronavirus entry

Field code: Cell biology/drug discovery

Keywords: SARS-CoV-2, coronavirus, COVID-19, viral entry, endocytosis, drug repurpose screen, heparan sulfate proteoglycans/HSPGs, actin cytoskeleton, Tilorone, Mitoxantrone, Raloxifene

Drugs capable of blocking the infectious cycle of the coronavirus SARS-CoV-2 are urgently needed to tackle the ongoing COVID-19 pandemic. To this end, the cell entry of SARS-CoV-2, initiated by the binding of the viral Spike (S) protein to human ACE2, has emerged as an attractive drug repurposing target. Here we use murine leukemia viruses pseudotyped with Spike from SARS-CoV or SARS-CoV-2 to demonstrate that ACE2-mediated coronavirus entry can be mitigated by heparin, a heparan sulfate-related glycan, or by genetic ablation of biosynthetic enzymes for the cell surface heparan sulfate proteoglycans (HSPGs). A drug repurposing screen targeting HSPG-dependent endocytosis identifies pharmacologically active endocytosis inhibitors that also abrogate coronavirus cell entry. Among them, Mitoxantrone (EC_{50}=~10 nM) targets HSPGs directly, whereas Sunitinib and BNTX disrupt the actin network to impair HSPG-assisted viral entry. Gene expression profiling suggests potential combination regimens that optimally target HSPG-dependent viral entry. Altogether, our study establishes HSPGs as an assisting factor for ACE2 in endocytosis-mediated coronavirus entry and identifies drugs that can be repurposed to target this important stage in the viral life cycle.

The ongoing pandemic of the coronavirus disease 2019 (COVID-19) has claimed more than half-a-million lives and severely damaged the global economy. This severe acute respiratory syndrome (SARS) is caused by a novel coronavirus SARS-CoV-2 (*1, 2*), which is closely related to SARS-CoV, the virus underlying the 2003 SARS outbreak (*3*). As a positive-sense, single-stranded RNA virus bearing a membrane envelope, coronavirus enters cells when this membrane envelope fuses with host membranes (*4*). Previous studies showed that the entry of SARS-CoV is primarily mediated by ACE2-dependent endocytosis (*5, 6*), and new evidence suggests that SARS-CoV-2 may follow the same entry path (*1, 7*). Specifically, limiting the production of phosphatidylinositol 4,5-bisphosphate (PIP2) inhibits the fusion of the SARS-CoV-2 envelop with the endolysosomes and subsequent viral entry (*8, 9*). Additionally, entry-associated membrane fusion requires several host proteases, including the lysosome-localized Cathepsin B/L and TMPRSS2 (*10-12*). The fact that increasing the lysosomal pH in either TMPRSS2 positive Caco-2 or TMPRSS2 negative HEK293 cells both significantly inhibits SARS-CoV-2 cell entry (*10*) also suggests the endolysosome as a major entry site for SARS-CoV-2.

Our previous study on the intercellular transmission of misfolded α-Synuclein (α-Syn) fibrils, a cellular process reminiscent of viral infection, revealed an endocytosis mechanism by which the cell surface heparan sulfate proteoglycans (HSPGs) facilitate receptor-mediated uptake of protein assemblies bearing excess positive charges (*13*). Strikingly, this mechanism can be co-opted by certain viruses and pathogens to establish productive infection (*13, 14*). To identify drugs that can diminish the spreading of misfolded α-Syn and the associated Parkinsonism (*15*), we screened and found eight FDA-approved drugs that block the endocytosis of preformed α-Syn fibrils (see below). Intriguingly, one of the candidates Tilorone, was recently reported as an inhibitor for SARS-CoV-2 infection (*16*). This coincidence, together with reports that the SARS-

CoV-2 Spike can interact with heparin (*17, 18*) and that treating cells with heparinase or heparin inhibits SARS-CoV cell entry (*19*) prompted us to investigate the possibility of targeting HSPG-dependent endocytosis as a COVID-19 therapeutic strategy.

Heparin or knockdown of *HSPG biosynthetic enzymes* mitigates ACE2-mediated coronavirus entry

To study coronavirus cell entry, we used luciferase-expressing pseudoviral particles (PPs) bearing SARS-CoV or SARS-CoV-2 Spike to infect Calu-3 (human lung epithelial cells positive for TMPRSS2) or HEK293T (human embryonic kidney cells negative for TMPRSS2) cells. Incubating cells with PPs resulted in luciferase expression consistently higher than the background (non-infected cells), although the increase was at most modest. By contrast, in HEK293T cells stably expressing ACE2-GFP, transduction with SARS-CoV or SARS-CoV-2 PPs resulted in luciferase expression ~170-fold higher than the background (Fig. S1A-D). These results suggest that these PPs use an ACE2-dependent mechanism to enter cells, and thus establish Calu-3 and ACE-GFP cells as relevant models representing cells with different sensitivity to infection.

To investigate the role of HSPGs in coronavirus entry, we first treated Calu-3 or ACE2-GFP cells with heparin, a Spike-binding glycan structurally related to heparan sulfate in HSPG (Figure 1A). For experiments in Calu-3 cells, we monitor cell viability in the absence of viral transduction as a control for compound cytotoxicity. In ACE-GFP cells, ACE-GFP expression was used to control the confounding factors such as drug effects on gene expression or cell growth (Figure 1B). Heparin treatment did not significantly induce cytotoxicity (Data not shown), but dose-dependently mitigated the luciferase signals associated with the entry of both SARS-CoV and SARS-CoV-2 PPs, with a more significant effect on SARS-CoV (Figure 1C). This phenotype

correlated inversely with the affinity of ACE2 to the Spike proteins from these viruses (*12, 20, 21*). Likewise, heparin also reduced luciferase expression in SARS-CoV or SARS-CoV-2-treated ACE2-GFP cells (Figure 1D). Although the level of inhibition was lower in ACE2-GFP cells than in Calu-3 cells, a similar differential effect on the two viruses was observed. These data support a model in which heparin competitively inhibits coronavirus entry, but at sub-maximum inhibition, this effect could be offset by the increased affinity of Spike to ACE2 or by increased ACE2 expression.

Next, we used small interfering RNA (siRNA) or CRISPR to disrupt genes encoding HSPG biosynthetic enzyme XYLT2 and SLC35B2 (Figure 1E, Fig. S1E-G). *XYLT2* encodes one of the two HSPG chain initiation enzymes, whereas SLC35B2 is a Golgi-localized transporter for 3'-phosphoadenosine 5'-phosphosulfate (PAPS), which is essential for chain sulfation (*22*). Knockdown of *XLYT2* by ~80% differentially inhibited SARS-CoV and SARS-CoV-2 PP entry similarly as heparin treatment (Figure 1F). By contrast, CRISPR-mediated inactivation of *SLC35B2* inhibited the entry of SARS-CoV and SARS-CoV-2 more dramatically, but to a similar level (Figure 1G,). Analyses of GFP fluorescence in cell extracts showed no effect of *SCL35B2* deficiency on ACE2-GFP expression (Fig. S1H). Nevertheless, knockout of *SLC35B2* significantly abolished the binding of SARS-CoV-2 PPs to ACE2-GFP cells (Figure 1H, I). Altogether, these results support a model in which HSPGs serve as a virus-recruiting factor to assists ACE2 in coronavirus cell entry.

A drug repurposing screen identifies inhibitors of HSPG-dependent endocytosis

HSPGs, as negatively charged biopolymers, can recruit ligands bearing positive charges to the cell surface to promote their endocytosis (*14*). Our interest in drugs capable of reducing HSPG-

dependent uptake of α-Syn filamentous inclusions led us to a quantitative high-throughput screen (qHTS) (Fig. S2A), which identified 8 approved drugs that inhibited α-Syn fibril uptake in both HEK293T cells and primary neurons (Figure 2A, Fig. S2B-D). Among them, Tilorone, a previously established antiviral agent (*23*) not only reduced α-Syn fibril uptake in mouse hippocampal neurons, but also diminished fibril-induced endogenous α-Syn phosphorylation (Fig. S2E-H), a pathologic hallmark of Parkinson's disease (*24*).

Additional studies using a panel of endocytosis cargos showed that the identified drugs are endocytosis inhibitors with a preference for HSPG ligands. Among the cargos tested, supercharged GFP (GFP+), polycation-coated DNA, and VSVG-pseudotyped lentivirus all enter cells via a *SLC35B2* dependent mechanism (*13*), whereas Transferrin uses a HSPG independent but clathrin-dependent endocytosis pathway. The cholera toxin B chain (CTB) reaches the Golgi apparatus via a clathrin-independent mechanism (*25*). None of the drugs affected the internalization of CTB, but Sunitinib and BNTX appeared to disrupt the perinuclear stacking of the Golgi system (Fig. S3A, B). These drugs also had little impact on Transferrin endocytosis (Fig. S3C), but they could reduce the uptake of HSPG cargos to various levels (Figure 2B, Fig. S3D-F) with Mitoxantrone being the most potent one: at 5 μM, it almost completely blocked the endocytosis of all HSPG cargos tested (Figure 2B).

Drugs targeting HSPG-dependent endocytosis inhibit coronaviral entry

We next tested whether the identified endocytosis inhibitors could block ACE2-mediated PP entry. Indeed, when present during transduction, most of these drugs (except for Exifone and K114) could significantly reduce the entry of both SARS-CoV and SARS-CoV-2 PPs at doses that did not impose significant cytotoxicity (Figure 2C-F, Fig. S4A-D). Additional studies done with

infectious SARS-CoV-2 in Vero E6 cells showed that several drugs (Raloxifene, BNTX, and K114) could reduce the cytopathic effect (CPE) caused by the virus. As expected, this phenotype was only seen at low doses due to the intrinsic cytotoxicity of the drugs at high doses. One exception is Tilorone, which did not show much cytotoxicity at the tested concentrations, but dose-dependently protected Vero E6 cells from virus-induced cytopathic effect (CPE) (Figure 4G, H, Fig. S4E, F). Together, these results show that inhibitors targeting HSPG-dependent endocytosis can also affect the entry of coronavirus, further corroborating the notion that HSPGs assist ACE2 in endocytosis-mediated coronavirus entry.

Mitoxantrone directly targets cell surface HSPGs

Among the tested drugs, Mitoxantrone is the strongest inhibitor for HSPG-dependent endocytosis. Mitoxantrone was previously discovered as a DNA intercalator, which also inhibits type II DNA topoisomerase (*26, 27*). Accordingly, Mitoxantrone is currently approved for treatment of acute non-lymphocytic leukemia, prostate cancer, and multiple sclerosis.

Because Mitoxantrone is a blue compound absorbing light at wavelength 620 nm and 685 nm (Figure 3A). we used this spectral property to trace its localization in drug-treated cells, which hinted at its cellular target. To this end, we performed subcellular fractionation using Mitoxantrone-treated cells to obtain the nucleus (1,000g pellet), mitochondria-enriched heavy membranes (7,000g pellet), light membranes (100,000g pellet), and cytosol (100,000g supernatant) fractions (Figure 3B, top panel). Although blue color was seen in every pellet fraction, Mitoxantrone in the nucleus and heavy membrane fraction was resistant to extraction by a buffer containing the non-ionic detergent NP40 or 1% SDS, probably due to tight association with DNA. By contrast, Mitoxantrone in the light membranes (containing the plasma membrane and

endoplasmic reticulum as demonstrated by immunoblotting, middle panel) could be readily released by an NP40-containing buffer and detected by a spectrometer (Figure 3B). No Mitoxantrone was detected in the cytosol fraction. Thus, in addition to DNA, Mitoxantrone also binds to cell membranes.

Several lines of evidence suggest that Mitoxantrone inhibits endocytosis and viral entry by targeting the cell surface HSPGs. First, the amount of P100-associated Mitoxantrone from *SLC35B2* deficient cells was significantly lower than that of wild-type cells, which could be rescued by re-expression of SLC35B2 (Figure 3C). Thus, the binding of Mitoxantrone to light membranes appears to be in part mediated by HSPGs. Consistent with this interpretation, Mitoxantrone could readily bind to heparin beads but not to a Sepharose control (Figure 3D). Intriguingly, Banoxantrone, a structurally related drug, did not bind to heparin (Fig. S5), which suggests a specific and direct interaction between Mitoxantrone and heparin and explains the SLC35B2-dependent association of Mitoxantrone with cell membranes. Importantly, compared to Mitoxantrone, Banoxantrone failed to interact with cell membranes (Figure 3E), and coincidentally, it was much weaker to reduce SARS-CoV-2 PP entry into host cells (Figure 3F). Surprisingly, while several weaker inhibitors but not Mitoxantrone could rescued the CPE of SARS-CoV-2 in Vero E6 cells (Figure 2G, H, Fig. S4), which might be due to the relatively high cytotoxicity of Mitoxantrone. In this regard, it is compelling to see that the dose-dependent toxicity profiles of Mitoxantrone and Banoxantrone were indistinguishable (Figure 3G). The uncoupling of the antiviral and the anti-cancer activities of Mitoxantrone suggests the possibility of generating similar antiviral compounds with reduced cytotoxicity.

Sunitinib and BNTX disrupt actin dynamics to impair HSPG-dependent viral entry

The endocytosis of many HSPG-dependent cargos requires the actin cytoskeleton (*13*). We therefore determined whether the newly identified drugs affect the actin network using U2OS cells stably expressing Tractin-EGFP, an actin filament label (*28*). Confocal microscopy showed that most drugs did not change the actin network except for Sunitinib, an anti-cancer agent, and BNTX, an opioid receptor antagonist (Figure 4A, Fig. S6A). In untreated cells, actin monomers polymerize near peripheral membranes, forming a microfilament network with many parallel actin filaments (Fig. S6A). Additionally, a meshwork of actin is associated with the cell cortex, and thick actin bundles named stress fibers are often found near basal membranes. In cells exposed to Sunitinib, the actin microfilaments were frequently replaced by short disoriented actin segments. Many cells also contained an increased number of filopodia. By contrast, cells treated with BNTX had significantly reduced actin filaments, and many cells contained actin-bearing aggregates. These phenotypes were further confirmed by TIRF microscopy analysis of membrane-associated actin in drug-treated cells (Fig. S6B).

To further elucidate the mechanistic actions of Sunitinib and BNTX, we used live-cell imaging to monitor the acute changes in actin dynamics in drug-treated cells. Shortly after Sunitinib treatment, we observed extensive de novo actin filament formation (Figure 4B, C, Supplementary movies 2 vs. 1). Actin polymerization was also detected in the cell periphery where it drove filopodium formation (Figure 4B) but was not seen near basal membranes where stress fibers were located (Supplementary movie 4 vs. 3). Unlike Sunitinib, BNTX treatment caused actin filaments to disassemble in the peripheral cortex, resulting in rapid shrinking of actin microfilaments and the loss of membrane ruffling (Figure 4D, E, Supplementary movies 6 vs. 5). Together, these data suggest that Sunitinib promotes actin assembly to form disoriented filaments, while BNTX disrupts the cortex actin meshwork either by promoting actin disassembly or

inhibiting actin assembly. The fact that two structurally unrelated actin inhibitors both block coronavirus entry strongly suggests that the endocytosis of coronavirus requires the actin cytoskeleton. Accordingly, SARS-CoV-2 cell entry was also sensitive to Latrunculin A, a well-established actin inhibitor (Figure 4F). These findings, together with the fact that a previous drug screen identified Sunitinib as an entry inhibitor for Ebola virus (*29*), suggest that the actin network may paly a previously unappreciated role in the entry of many viruses into host cells.

Combination regimens target HSPG-assisted viral entry

Lastly, we used gene expression profile as a signature to distinguish the action of Tilorone, Raloxifene (a hormone therapy agent for bone loss), Piceatannol (an anti-inflammatory drug), and Mitoxantrone. We treated HEK293T cells with these drugs for 6 h at a dose that imposed a significant inhibition on viral entry. Differential gene expression analyses showed that Mitoxantrone had the most significant impact on gene expression (Figure 5A), consistent with its relatively high cytotoxicity. By contrast, Tilorone had the smallest effect, altering only a limited number of genes with small changes (Fig. S7A-D). Cluster analysis showed that the gene expression signature associated with Raloxifene treatment was more similar to that of Piceatannol-treated cells than to Tilorone- or Mitoxantrone-treated cells (Figure 5A), suggesting that Tilorone uses a mechanism distinct from the other drugs, therefore, raising the possibility of combining Tirolone with other drugs to achieve stronger inhibition of viral entry. Indeed, in our initial trial, while Tilorone by itself required high doses to inhibit SARS-CoV-2 PP entry, co-treatment with Sunitinib, BNTX, Raloxifene, or Piceatannol all significantly enhanced the inhibition of SARS-CoV-2 PP entry by Tilorone, while Mitoxantrone modestly increased Tilorone's activity (Figure

5B-F). Importantly, no synergy in cytotoxicity was observed between Tilorone and other drugs (Figure 5G).

While ACE2-mediated coronavirus entry into host cells is known to be controlled by a protease-dependent priming step (*10-12*), evidence presented here supports an additional layer of regulation by the cell surface HSPGs, which consist of two protein families (6 Glypicans and 4 Syndecans) (*22*). These proteins all bear negative charge-enriched heparan sulfate polymers that can promote the interaction of cells with a variety of endocytic ligands including viruses and pathogens (*14*). Our data suggest that HSPGs help to recruit SARS-CoV-2 to the cell surface, which should increase its local concentration for effectively engaging ACE2. Additionally, HSPGs might have a role downstream of viral recruitment given the observed binding of heparin to Spike, which induces a conformational change in the latter (*17*). Although our study focuses on coronavirus, drugs targeting HSPG-dependent endocytosis may have broad antiviral activities. Consistent with this view, Tilorone has long been recognized as a general antiviral agent outside the US. An early study in mice showed that Tilorone administrated orally might upregulate interferon production (*30*), but our gene expression study did not reveal significant changes in interferon expression by Tirolone. Instead, the demonstration of Tilorone as an endocytosis inhibitor offers an alternative explanation for its antiviral function. Importantly, our study also suggests that Tilorone, when combined with other endocytosis inhibitors can generate a promising anti-viral synergism. Thus, systematically testing combinations among drugs targeting different aspects of the coronaviral infectious cycle may offer a quick path to an effective treatment that benefits all COVID-19 patients.

References

1. P. Zhou *et al.*, A pneumonia outbreak associated with a new coronavirus of probable bat origin. *Nature* **579**, 270-273 (2020).
2. N. Zhu *et al.*, A Novel Coronavirus from Patients with Pneumonia in China, 2019. *N Engl J Med* **382**, 727-733 (2020).
3. K. V. Holmes, SARS-associated coronavirus. *N Engl J Med* **348**, 1948-1951 (2003).
4. M. Marsh, A. Helenius, Virus entry: open sesame. *Cell* **124**, 729-740 (2006).
5. H. Wang *et al.*, SARS coronavirus entry into host cells through a novel clathrin- and caveolae-independent endocytic pathway. *Cell Res* **18**, 290-301 (2008).
6. C. Burkard *et al.*, Coronavirus cell entry occurs through the endo-/lysosomal pathway in a proteolysis-dependent manner. *PLoS Pathog* **10**, e1004502 (2014).
7. O. O. Glebov, Understanding SARS-CoV-2 endocytosis for COVID-19 drug repurposing. *FEBS J*, (2020).
8. X. Ou *et al.*, Characterization of spike glycoprotein of SARS-CoV-2 on virus entry and its immune cross-reactivity with SARS-CoV. *Nat Commun* **11**, 1620 (2020).
9. Y. L. Kang *et al.*, Inhibition of PIKfyve kinase prevents infection by EBOV and SARS-CoV-2. *bioRxiv*, (2020).
10. M. Hoffmann *et al.*, SARS-CoV-2 Cell Entry Depends on ACE2 and TMPRSS2 and Is Blocked by a Clinically Proven Protease Inhibitor. *Cell* **181**, 271-280 e278 (2020).
11. M. Hoffmann, H. Kleine-Weber, S. Pohlmann, A Multibasic Cleavage Site in the Spike Protein of SARS-CoV-2 Is Essential for Infection of Human Lung Cells. *Mol Cell* **78**, 779-784 e775 (2020).
12. J. Shang *et al.*, Cell entry mechanisms of SARS-CoV-2. *Proc Natl Acad Sci U S A* **117**, 11727-11734 (2020).
13. Q. Zhang *et al.*, A myosin-7B-dependent endocytosis pathway mediates cellular entry of alpha-synuclein fibrils and polycation-bearing cargos. *Proc Natl Acad Sci U S A* **117**, 10865-10875 (2020).
14. H. C. Christianson, M. Belting, Heparan sulfate proteoglycan as a cell-surface endocytosis receptor. *Matrix Biol* **35**, 51-55 (2014).
15. R. J. Karpowicz, Jr., J. Q. Trojanowski, V. M. Lee, Transmission of alpha-synuclein seeds in neurodegenerative disease: recent developments. *Lab Invest* **99**, 971-981 (2019).
16. S. Jeon *et al.*, Identification of antiviral drug candidates against SARS-CoV-2 from FDA-approved drugs. *Antimicrob Agents Chemother*, (2020).
17. C. Mycroft-West *et al.*, The 2019 coronavirus (SARS-CoV-2) surface protein (Spike) S1 Receptor Binding Domain undergoes conformational change upon heparin binding. *bioRxiv*, (2020).
18. S. Kim *et al.*, Characterization of heparin and severe acute respiratory syndrome-related coronavirus 2 (SARS-CoV-2) spike glycoprotein binding interactions. *Antiviral Research*, (2020).
19. J. Lang *et al.*, Inhibition of SARS pseudovirus cell entry by lactoferrin binding to heparan sulfate proteoglycans. *PLoS One* **6**, e23710 (2011).
20. J. Shang *et al.*, Structural basis of receptor recognition by SARS-CoV-2. *Nature* **581**, 221-224 (2020).

21. D. Wrapp *et al.*, Cryo-EM structure of the 2019-nCoV spike in the prefusion conformation. *Science* **367**, 1260-1263 (2020).
22. S. Sarrazin, W. C. Lamanna, J. D. Esko, Heparan sulfate proteoglycans. *Cold Spring Harb Perspect Biol* **3**, (2011).
23. S. Ekins, P. B. Madrid, Tilorone, a Broad-Spectrum Antiviral for Emerging Viruses. *Antimicrob Agents Chemother* **64**, (2020).
24. H. Fujiwara *et al.*, alpha-Synuclein is phosphorylated in synucleinopathy lesions. *Nat Cell Biol* **4**, 160-164 (2002).
25. N. L. Wernick, D. J. Chinnapen, J. A. Cho, W. I. Lencer, Cholera toxin: an intracellular journey into the cytosol by way of the endoplasmic reticulum. *Toxins (Basel)* **2**, 310-325 (2010).
26. J. Kapuscinski, Z. Darzynkiewicz, Interactions of antitumor agents Ametantrone and Mitoxantrone (Novatrone) with double-stranded DNA. *Biochem Pharmacol* **34**, 4203-4213 (1985).
27. M. D. Crespi, S. E. Ivanier, J. Genovese, A. Baldi, Mitoxantrone affects topoisomerase activities in human breast cancer cells. *Biochem Biophys Res Commun* **136**, 521-528 (1986).
28. M. Melak, M. Plessner, R. Grosse, Actin visualization at a glance. *J Cell Sci* **130**, 525-530 (2017).
29. J. Kouznetsova *et al.*, Identification of 53 compounds that block Ebola virus-like particle entry via a repurposing screen of approved drugs. *Emerg Microbes Infect* **3**, e84 (2014).
30. G. D. Mayer, R. F. Krueger, Tilorone hydrochloride: mode of action. *Science* **169**, 1214-1215 (1970).

Acknowledgements

We thank Susan Buchanan, Martin Gellert (NIDDK), and Liqiang Chen (University of Minnesota) for critical reading of the manuscript. The plasmids and protocols for pseudotyped particle generation were kind gifts from Dr. Gary Whittaker at Cornell University. The work is supported by the Intramural Research Program of the National Institute of Diabetes, Digestive & Kidney Diseases and of the National Center for Advancing Translational Sciences in the National Institutes of Health.

Author contribution

Q. Zhang, M. Swaroop, W. Zheng, and Ye, Y. designed the drug screen, Q. Zhang, C. Chen, Y. Xu, W. Zheng, and Ye Y. conceived the project, designed the study, and analyzed the data. Q.

Zhang, M. Swaroop, M. Pradhan, M. Xu, L. Wang, J. Lee, M. Shen, Z. Luo, W. Huang, and Y. Ye conducted the experiments. Y. Ye wrote the manuscript. All authors contribute to the editing of the manuscript.

Competing financial interests

The authors declare no competing financial interests.

Data Availability.

All data, associated protocols, methods, and sources of materials can be accessed in the main text or supplementary information. The mRNA sequencing data has been deposited to NCBI Sequence Read Archive. The accession ID is : PRJNA645209.

List of Supplementary materials:

Materials and Methods

Table S1

Figures S1-S7

Movies S1-S6

References (1-4)

Figure 1

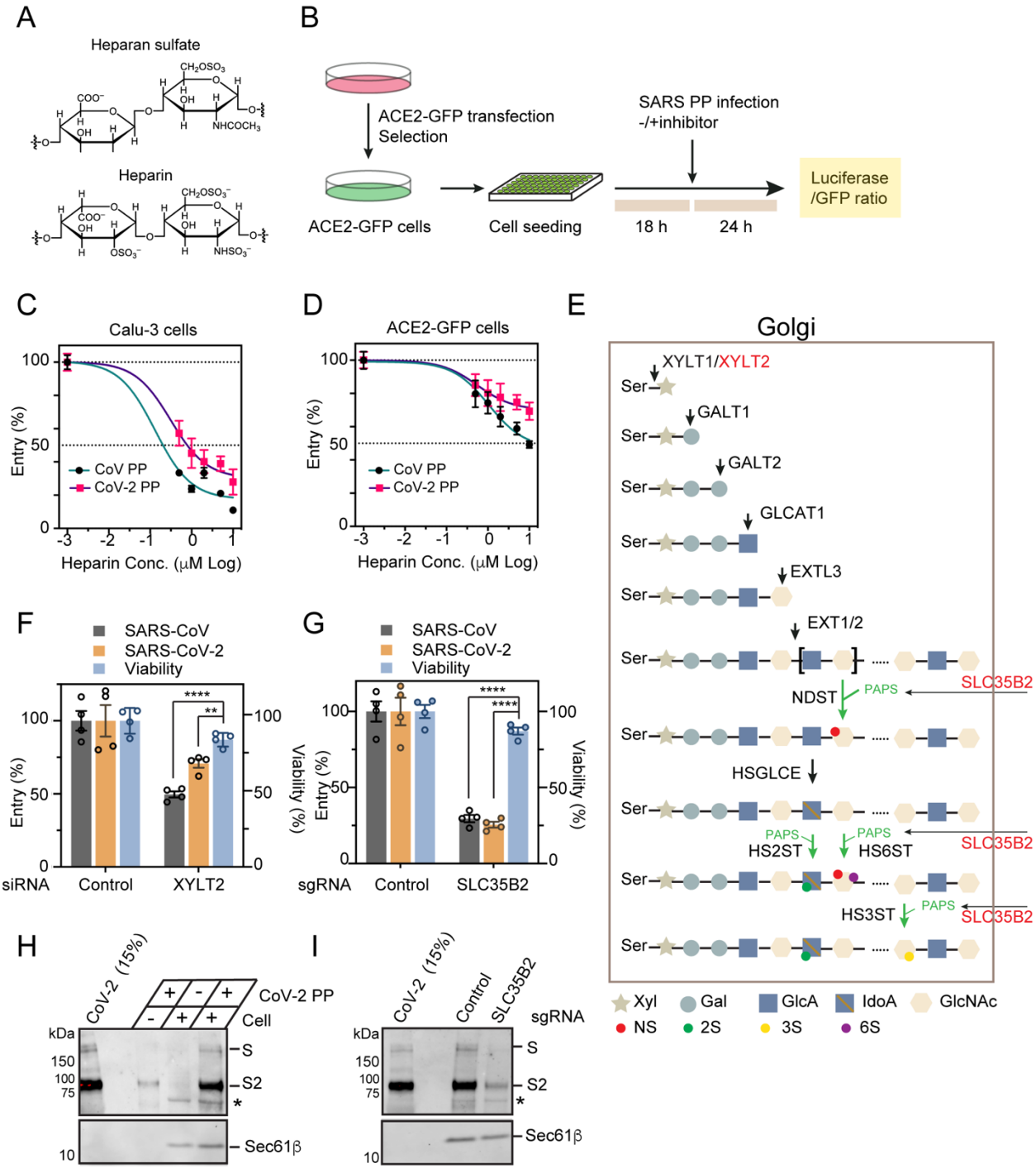

Figure 1 HSPGs facilitate ACE2-mediated entry of SARS-CoV and SARS-CoV-2.

(**A**) The chemical structures of heparan sulfate and heparin.

(**B**) The experimental scheme for inhibitor testing.

(**C**) Heparin competitively mitigates the entry of SARS-CoV and SARS-CoV-2 pseudoviral particles (PP). Calu-3 cells were transduced with SARS-CoV and SARS-CoV-2 PPs in the presence different heparin concentrations. The luciferase expression 48 h post-transduction indicates viral entry. Error bars indicate SEM, N=4.

(**D**) As in C, except that ACE2-GFP HEK293T cells were used.

(**E**) The HSPG biosynthetic pathway. Genes chosen for knockdown or knockout (KO) are in red.

(**F**) Knockdown of *XYLT2* reduces SARS-CoV and SARS-CoV-2 PP entry. ACE2-GFP cells transfected with either control or *XYLT2* siRNA were transduced with SARS-CoV or SARS-CoV-2 PPs for 24 h before the ratio of luciferase/GFP was determined. A parallel experiment done without the virus provides a control for the effect of gene knockdown on cell viability. Error bars indicate SEM, N=4. **, $p<0.01$, ****, $p<0.0001$ by unpaired Student t-test.

(**G**) *SCL35B2* is required for SARS-CoV and SARS-CoV-2 cell entry. As in F, except that control or *SLC35B2* CRISPR KO cells were used.

(**H** and **I**) *SLC35B2* promotes efficient binding of SARS-CoV-2 PPs to cells. (H) ACE2-GFP cells were spin-infected at 4 °C for 1h as indicated. After washing, virus bound to the cells was detected by immunoblotting. (I) The binding of SARS-CoV-2 PPs to control and *SLC35B2* deficient cells was analyzed by immunoblotting. S and S2 indicate full length and the protease-cleaved S2 domain, respectively. *, non-specific band.

Figure 2

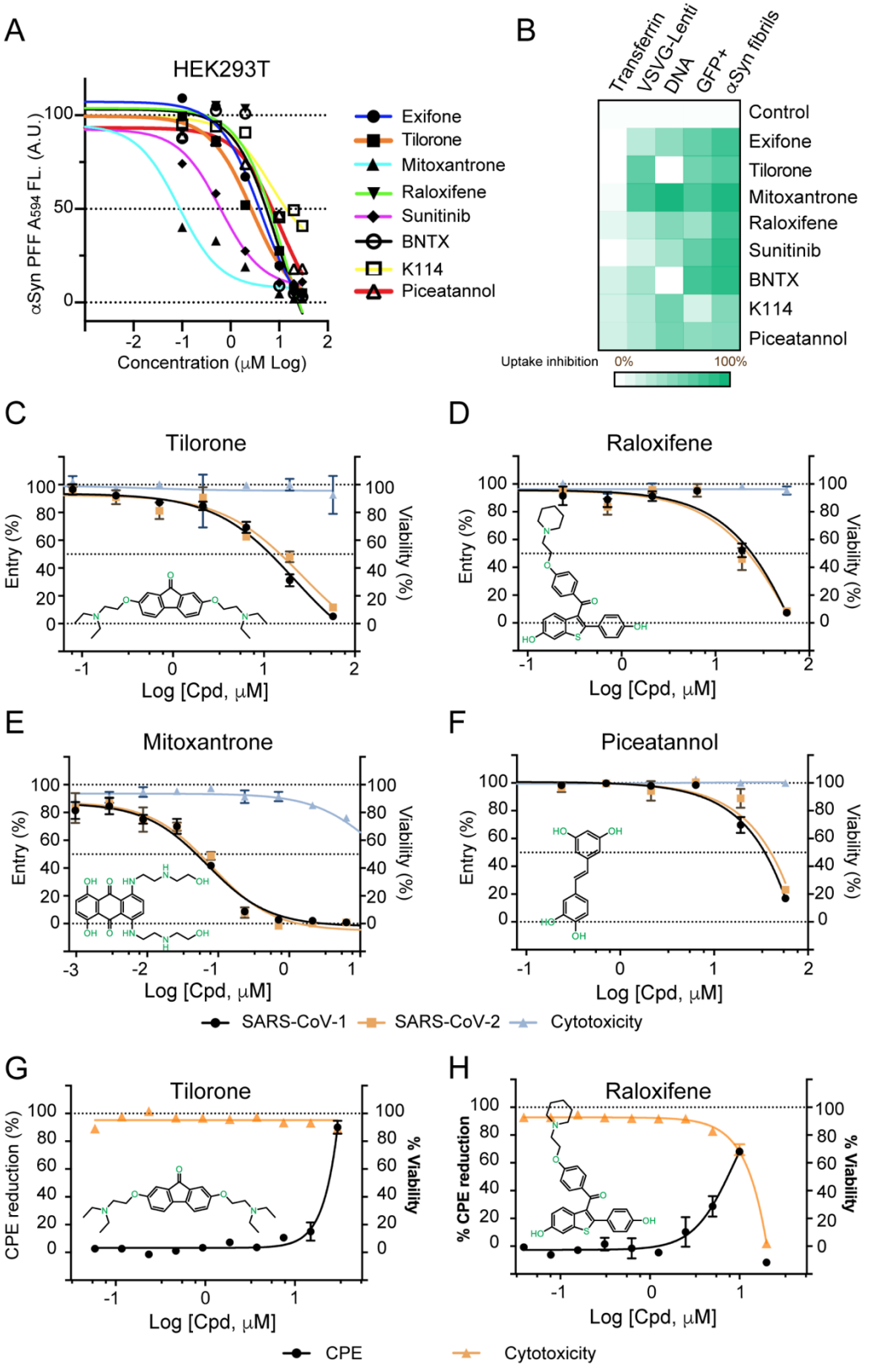

Figure 2 Drugs targeting HSPG-dependent endocytosis also mitigate coronavirus entry.

(**A**) Dose dependent inhibition of pHrodo red-labeled α-Syn fibril uptake. HEK293T cells were incubated with 400 nM pHrodo red-labeled α-Syn fibrils for 3 h in the presence of the indicated drugs. The integrated fluorescence (FL) signals were determined by flow cytometry.

(**B**) A heat map summary of the endocytosis inhibitory activities for the indicated drugs. All drugs were tested at 10 μM except for Sunitinib and Mitoxantrone (5 μM each). See Supplementary Figure 3 for details.

(**C**-**F**) Inhibition of SARS-CoV and SARS-CoV-2 PP entry by HSPG endocytosis inhibitors. HEK293 cells stably expressing ACE2-GFP were incubated with SARS-CoV or SARS-CoV-2 PPs in the presence of the indicated drugs. Percent of PP entry was determined by the luciferase level. Cells treated with the inhibitors without the PPs were used to determine drug cytotoxicity. Shown is a representative experiment from two independent repeats with similar results. Cpd, Compound. Error bars indicate SEM, N=4.

(**G** and **H**) Tilorone and Raloxifene protects Vero E6 cells from SARS-CoV-2-induced cytotoxicity. Viability of Vero E6 cells were measured after treatment with the indicated drugs in the presence of SARS-CoV-2 (black curves) or without the virus (orange curves). (CPE, Cytopathic effect). Error bars indicate SEM, N=2.

Figure 3

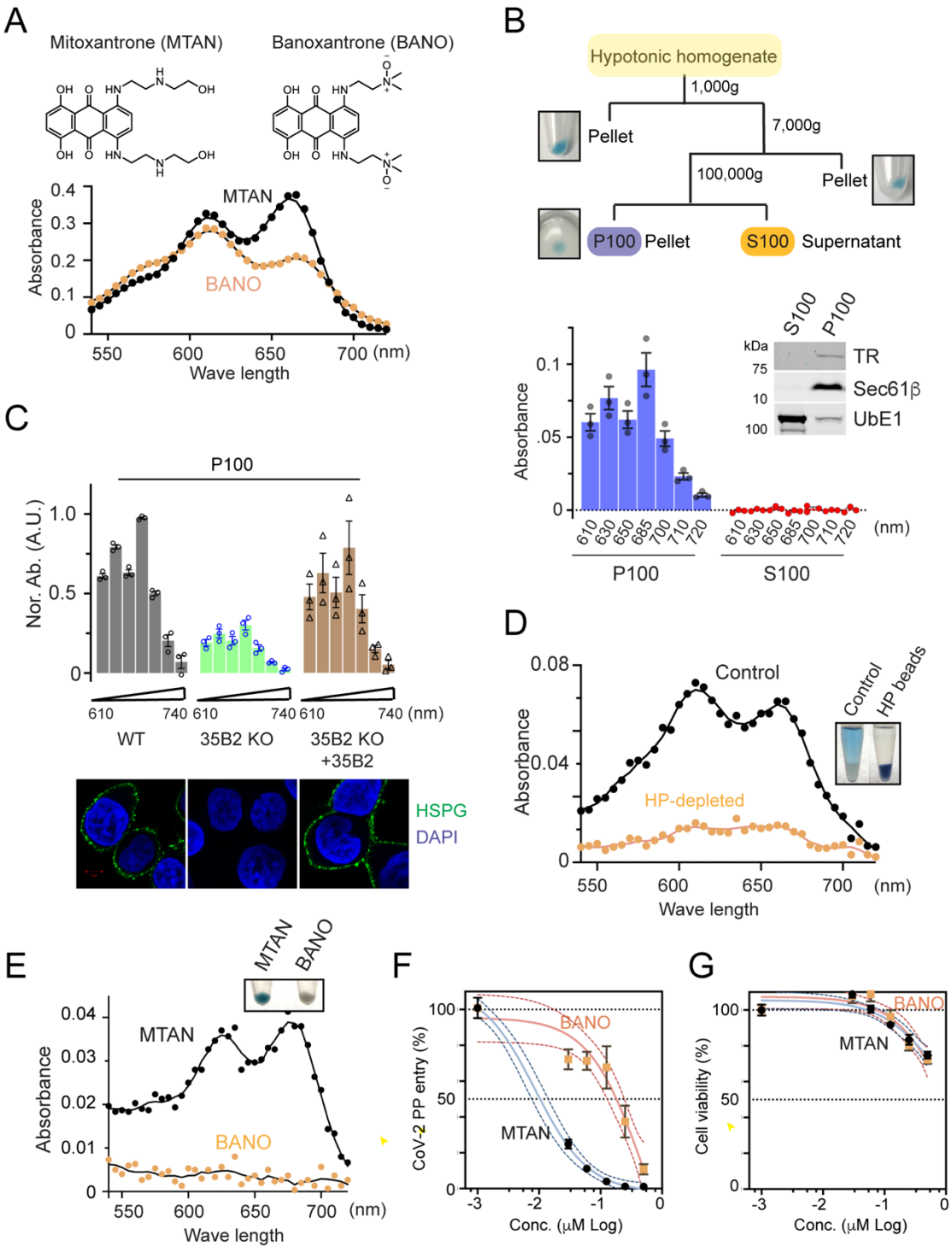

Figure 3 Mitoxantrone directly targets HSPGs on the cell surface.

(A) The chemical structures and absorbance spectra of Mitoxantrone (MTAN) and Banoxantrone (BANO).

(B) The subcellular distribution of Mitoxantrone. The scheme illustrates the experimental procedure. HEK293T cells were treated with 5 μM Mitoxantrone for 30 min at 37 °C before fractionation. The membrane pellet (P100) and cytosol supernatant (S100) fractions were analyzed by immunoblotting and by a spectrometry at the indicated wavelengths. Error bars indicate SEM. N=3.

(C) The membrane association of Mitoxantrone depends on *SLC35B2 (35B2)*. Cells of the indicated genotypes were treated with 5 μM Mitoxantrone for 30 min at 37 °C and then fractionated as in B. The absorbances of the P100 fractions were measured. The absorbance of the control sample at 680 nm was used for normalization. Bottom panels show the cells stained with DAPI (blue) and GFP+ (green) to label DNA and HSPG (Green), respectively. Error bars indicate SEM. N=3.

(D) Mitoxantrone binds heparin Sepharose. Mitoxantrone (50 μM) was incubated with either control Sepharose or heparin (HP)-coated Sepharose for 5 min. The picture shows the samples after centrifugation. The graph shows the absorbance spectra of the supernatant fractions.

(E) Banoxantrone does not bind to cell membranes. Cells treated with either Mitoxantrone or Banoxantrone at 5 μM for 30 min were fractionated and the absorbance spectra of the P100 fractions were measured. The picture shows the cell pellets after treatment.

(F) Banoxantrone has reduced antiviral activity. ACE2-GFP cells were incubated with SARS-CoV-2 in the presence of the indicated drugs. Error bars indicate SEM. Dashed lines indicate 95% confidence interval. N=4.

(G) The cytotoxicity profiles or Mitoxantrone and Banoxantrone in ACE2-GFP-expressing HEK293T cells. Error bars indicate SEM. N=3.

Figure 4

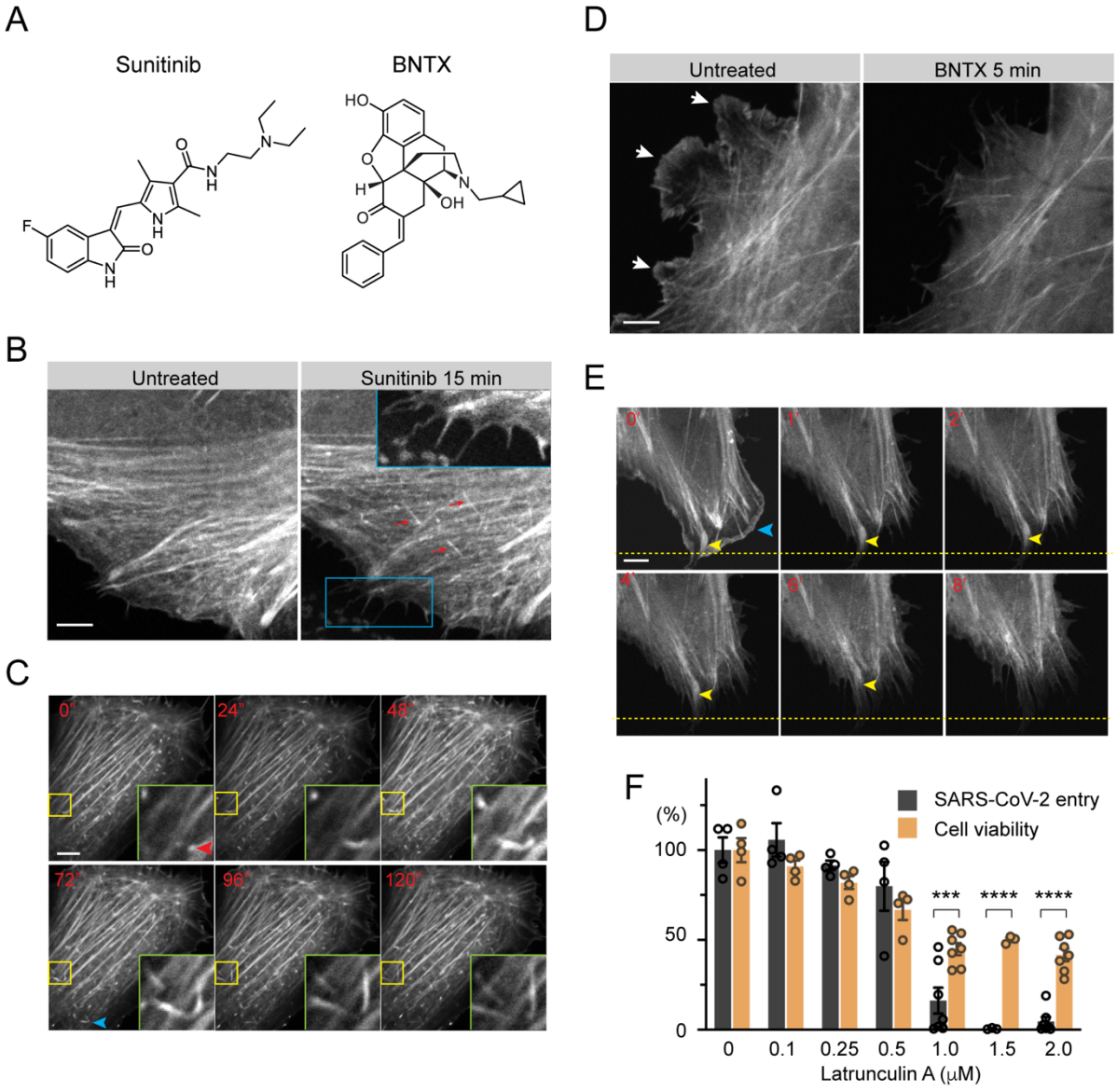

Figure 4 The actin cytoskeleton network is required for coronavirus entry.

(**A**) The chemical structures of Sunitinib and BNTX.

(**B** and **C**) Sunitinib stimulates actin filament formation at the cell periphery. (B) Confocal snapshots of a U2OS cell stably expressing Tractin-EGFP before or after Sunitinib (5 μM) treatment. The red arrows indicate new actin filaments formed in a direction perpendicular to the existing filaments. The inset shows an enlarged view of the box. (C) Live cell imaging of actin filament formation after Sunitinib treatment (5 μM, 60min). The arrows indicate examples of actin filament assembly. The insets show an enlarged view of the boxed areas. Scale bar, 5 μm.

(**D** and **E**) BNTX disrupts actin filaments at the cell periphery. (D) Confocal snapshots of a Tractin-EGFP cell before and after BNTX (10 μM) treatment. Arrows indicate the peripheral actin network disrupted by BNTX. (E) Live cell imaging shows the shrinking of peripheral membranes after BNTX treatment. Yellow arrowheads mark a retracting actin bundle.

(**F**) Latrunculin A inhibits SARS-CoV-2 entry. ACE2-GFP cells incubated with SARS-CoV-2 PPs in the presence of Latrunculin were analyzed for luciferase expression (Entry). A parallel treatment in the absence of the virus showed the effect of Latrunculin A on cell viability. Error bars indicate SEM. N=dot number. ***, $p<0.001$, ****, $p<0.0001$.

Figure 5

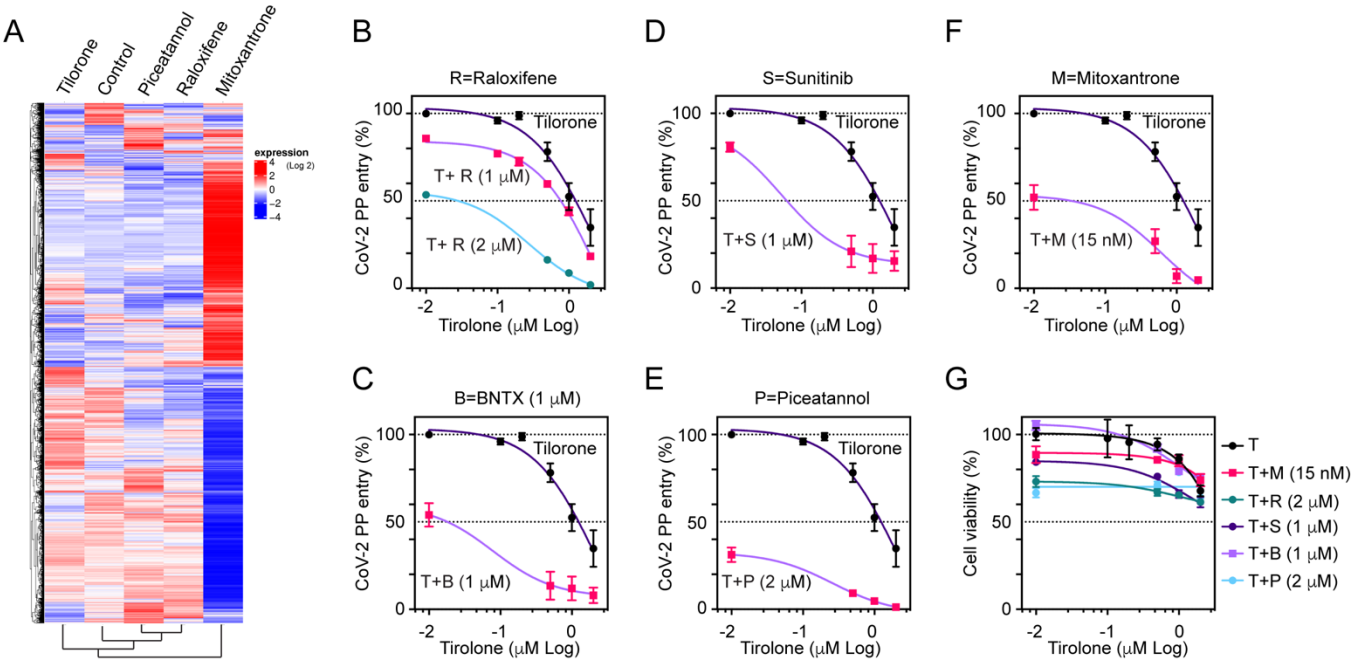

Figure 5 Exploring the combination regimens that optimally target ACE2-mediated coronaviral entry.

(**A**) A heatmap showing the gene expression profiles of untreated HEK293T cells or cells treated with the indicated drugs at 10 μM for 6 h (Mitoxantrone 5 μM).

(**B-F**) Results from a drug combination study. HEK293T-ACE2-GFP cells were incubated with SARS-CoV-2 PPs in the presence of different concentrations of Tilorone (T) either alone or together with a second drug as indicated. The ratio of luciferase/GFP from untreated cells was normalized as 100% viral entry. Error bars indicate SEM. N=4.

(**G**) A parallel treatment in the absence of virus shows drug-associated cytotoxicity. Error bars indicate SEM. N=4.

Supplementary Information

Materials and Methods

Chemicals

The initial screening library LOPAC^{R1280} was purchased from Sigma. The chemicals for the follow-up studies were purchased as indicated in the table below. Standard quality control by HPLC was conducted before the drugs were used in the study. Other chemicals and reagents were also listed in the table below.

Cell line, transfection, lentivirus production, and infection

HEK293T cells stably expressing human ACE2 tagged with GFP (ACE2-GFP) were generated by transfecting cells with pCMV-ACE2-GFP (Covex), and stable clones were hand-picked after neomycin (1 mg/ml) selection for 1 week. Two ACE2-GFP cell lines using either HEK293 or HEK293T as the parental line were independently generated and used at NCATS and NIDDK, respectively. U2OS cells stably expressing Clathrin light chain-mCherry and Tractin-EGFP and the CRISPRv2 construct expressing sgRNA targeting *SLC35B2* were described previously (*1*). Calu-3 cells were purchased from ATCC and maintained in MEM with 10% fetal bovine serum. sgRNA-expressing lentiviruses were produced by transfecting 1 million 293FT cells (Thermo Fisher Scientific) in a 3.5 cm dish with 0.4 μg pVSV-G, 0.6 μg psPAX2, and 0.8 μg CRISPRv2-sgRNA. Transfected cells were incubated with 3 ml fresh DMEM medium for 72 h before viruses were harvested.

α-Synuclein fibrils uptake assay

Fluorescence dye labeled α-Syn preformed fibrils were generated as previously described (*1*). α-Syn fibril uptake and phosphorylated α-Syn induction in primary neurons was performed as follows. Primary hippocampal neuron cultures were prepared from P0-1 murine pups. Hippocampi were dissected in Hanks' balanced salt solution (HBSS) and washed with MEM (Gibco) twice. The hippocampi were incubated with 0.25% trypsin (Gibco) containing 100 µg/mL DNase-I (Sigma) for 10 min at 37 °C. Trypsin was then inactivated by addition of MEM containing 10% FBS. After washing with MEM three times, the hippocampal cells were dissociated by pipetting several times in MEM containing 100 µg/mL DNase-I. Cells were centrifuged at 300 g for 5 min, and then resuspended in the plating medium (MEM containing 10% FBS, 1 mM sodium pyruvate (Sigma), 2 mM L-glutamine (Sigma), 100 µg/mL Primocin (Invitrogen) and 0.6% glucose). The cell solution was passed through a 70 µm strainer (VWR) once to filter out cell clumps. Cells were seeded into 24 well plates pre-coated with poly-D-lysine (50 µg/ml) and laminin (2 µg/mL). Generally, hippocampal cells obtained from 4 pups are needed to seed one 24-well plate. After incubation at 37 °C with 5% CO_2 for 24 h, the culture medium was changed to a neurobasal medium containing 2% B27 (Thermo Fisher), 0.5 mM L-glutamine and 100 µg/mL Primocin) to support the growth of hippocampal neurons. For α-Syn fibril treatment, the medium at D.I.V. 7-9 was replaced with fresh neuronal culture medium containing α-Syn PFF (400 nM). 14 days later, cells were stained with phosphor-Synuclein antibodies followed by a fluorescence-labeled secondary antibody together with DAPI. Cells were imaged by a LSM780 confocal microscope (Zeiss). siRNA-mediated gene silencing was performed by lipofectamine RNAiMAX (Invitrogen) mediated transfection following the instruction from the manufacture.

Identification of inhibitors targeting HSPG-dependent endocytosis.

HEK293T cells were seeded in white 1,536-well microplates that have transparent bottom (Greiner BioOne) at 2,000 cells/well in 2 µL media and incubated at 37 °C overnight (~16 h). pHrodo red-labeled α-Syn fibrils were added at 400 nM final concentration to each well by a dispenser. After 1 h incubation, compounds from the LOPAC^{R1280} library (Sigma) were titrated 1:3 in DMSO and dispensed via pintool at 23 nl/well to the assay plates. After 24 hours of incubation, the fluorescence intensity of pHrodo red was measured by a CLARIOstar Plus plate reader (BMG Labtech). Data were normalized using cells containing 400 nM pHrodo red-labeled Syn fibrils as 100% and medium containing 400 nM preformed fibrils-pHrodo red as 0%.

SARS-CoV and SARS-CoV-2 pseudotyped particles (PP)

SARS-CoV-S, SARS-CoV2-S, and ΔEnv (lack the Spike protein) pseudotyped particles (PPs) were custom manufactured by the Codex Biosolutions (Gaithersburg, MD) following previously reported methods using a murine leukemia virus (MLV) pseudotyping system (*2, 3*). The SARS-CoV2-S construct with Wuhan-Hu-1 sequence (BEI #NR-52420) was C-terminally truncated by 19 amino acids to reduce ER retention for pseudotyping (*4*).

PP entry assay in the 1536-well format

HEK293-ACE2 cells seeded in white, solid bottom 1536-well microplates (Greiner BioOne) at 2,000 cells/well in 2 µL medium were incubated at 37 °C with 5% CO2 overnight (~16 h). Compounds were titrated 1:3 in DMSO and dispensed via pintool at 23 nl/well to the assay plates. Cells were incubated with compounds for 1 h at 37 °C with 5% CO_2 before 2 µl/well of PPs were added. The plates were then spinoculated by centrifugation at 1,500 rpm (453 x g) for 45 min and incubated for 48 h at 37 °C 5% CO2 to allow cell entry of PPs and the expression of luciferase.

After the incubation, the supernatant was removed with gentle centrifugation using a Blue Washer (BlueCat Bio). Then 4 μL/well of Bright-Glo luciferase detection reagent (Promega) was added to assay plates and incubated for 5 min at room temperature. The luminescence signal was measured using a PHERAStar plate reader (BMG Labtech). Data were normalized with wells containing PPs as 100% and wells containing control ΔEnv PP as 0%. Experiments shown in Figure 2C-F, Fig. S4A-D were conducted in this format by NCATS.

PP entry assay in the 96-well format

HEK293T-ACE2-GFP cells were seeded in white, transparent bottom 96-well microplates (Thermo Fisher Scientific) at 20,000 cells per well in 100 μl growth medium and incubated at 37 °C with 5% CO2 overnight (~16 h). The growth medium was carefully removed and 50 μl PPs or PPs containing compounds were added into each well. The plates were then spinoculated by centrifugation at 1500 rpm (453 x g) for 45 min and incubated for 24h (48 h for Calu-3 cells) at 37 °C 5% CO_2 to allow cell entry of PPs and the expression of luciferase. After incubation, the supernatant was carefully removed. Then 50 μl/well of Bright-Glo luciferase detection reagent (Promega) was added to assay plates and incubated for 5 min at room temperature. The luminescence signal was measured by a Victor 1420 plate reader (PerkinElmer). For ACE2-GFP cells, the GFP signal was also determined by the plate reader. Data were normalized with wells containing PPs but no compound as 100%, and wells mock-treated with phosphate buffer saline (PBS) as 0%, and the ratio of luciferase to the corresponding GFP intensity was calculated. We noticed that the drug potency measured in the ACE2-expressing cells by the 96-well format is ~6-10-fold higher than that from the 1,536 formats, which is probably due to the longer incubation required for the 1,536 formats. Under this condition, the drugs might lose activities due to cell

metabolism or decomposing. The difference in the cell lines may also contribute to the discrepancy. Experiments shown in Figure 1C, D, F, G, Figure 3F, G, Figure 4F, Figure 5B-G were done following this protocol at NIDDK.

ATP content cytotoxicity assay in the 1536-well format

HEK293-ACE2 cells were seeded in white, solid bottom 1,536-well microplates (Greiner BioOne) at 2,000 cells/well in 2 µl medium and incubated at 37 °C with 5% CO2 overnight (~16 h). Compounds were titrated 1:3 in DMSO and dispensed via pintool at 23 nl/well to assay plates. Cells were incubated for 1 h at 37 °C 5% CO2 before 2 µl/well of media was added. The plates were then incubated at 37 °C for 48 h at 37C 5% CO2. After incubation, 4 µl/well of ATPLite (PerkinElmer) was added to assay plates and incubated for 15 min at room temperature. The luminescence signal was measured using a Viewlux plate reader (PerkinElmer). Data were normalized with wells containing cells as 100%, and wells containing media only as 0%.

ATP content cytotoxicity assay in the 96-well format

HEK293T-ACE2-GFP cells were seeded in white, transparent bottom 96-well microplate (Thermo Fisher Scientific) at 20,000 cells per well in 100 µl/well growth medium and incubated at 37 °C with 5% CO2 overnight (~16 h). The growth medium was carefully removed and 100 µl medium with compounds was added into each well. The plates were then incubated at 37 °C for 24 h (48 h for Calu3 cells) at 37 °C 5% CO2. After incubation, 50 µL/well of ATPLite (PerkinElmer) was added to assay plates and incubated for 15 min at room temperature. The luminescence signal was measured using a Victor plate reader (PerkinElmer). Data were normalized with wells containing cells but no compound as 100%, and wells containing media only as 0%.

SARS-CoV-2 cytopathic effect (CPE) assay

SARS-CoV-2 CPE assay was conducted at the Southern Research Institute (Birmingham, AL) as fee-for-service. Briefly, compounds were titrated in DMSO and acoustically dispensed into 384-well assay plates at 60 nl/well. Cell culture medium (MEM, 1% Pen/Strep/GlutaMax, 1% HEPES, 2% HI FBS) was dispensed at 5 µl/well into assay plates and incubated at room temperature. Vero E6 (selected for high ACE2 expression) was inoculated with SARS CoV-2 (USA_WA1/2020) at 0.002 M.O.I. in media and quickly dispensed into assay plates at 4,000 cells/well in 25 µl volume. Assay plates were incubated for 72 h at 37 °C, 5% CO_2, 90% humidity. Then, 30 µl/well of CellTiter-Glo (Promega) was dispensed, incubated for 10 min at room temperature, and the luminescence signal was read on an EnVision plate reader (PerkinElmer). An ATP content cytotoxicity assay was conducted with the same protocol as CPE assay except that SARS-CoV-2 virus was omitted from the incubation.

GFP+ purification and HSPG staining

His-tagged GFP+ was reported previously (*1*). To stain the cell surface HSPG by GFP+, we incubated cells with 200 nM GPF+ in the growth medium on ice for 15min. Cells were then fixed and stained with DAPI to reveal the nucleus.

Endocytosis and viral binding assays

To test the effect of the compounds on DNA uptake, we seeded HEK293T cells previously infected with a YFP-expressing retrovirus at 0.2 x 10^6/well in a poly-lysine D coated 12 well plate. 24 h later, cells were treated with the chemicals for 30 min before a transfection mixture containing

0.2 µg mCherry-expressing plasmid and 0.6 µl TransIT293 (Mirus) was added to the cells. Cells were incubated with the DNA for 4 h, after which the medium was replenished. The cells were further grown for 48 h. Cells were then lysed in NP40 lysis buffer and the fluorescence intensity in cleared lysates was measured by a Fluoromax3 fluorometer (Horiba).

To test the effect of compounds on VSVG-coated lentivirus uptake/infection, HEK293T cells expressing YFP were seeded at $0.2x10^6$/well in a poly-lysine D coated 12 well plate. After 24 h, cells were treated with compounds for 30 min and then infected with a mCherry-expressing lentivirus at M.O.I. of ~ 2.0 in the presence of the compounds for 6 h. The virus and compounds were removed, and cells were further grown in fresh medium for 48 h before fluorescence measurement.

To test the effect of compounds on GFP+ or transferrin uptake, HEK293T cells were seeded at 25,000 cells per well in an 8 well chamber (ibidi). 24 h later, cells were treated with compounds for 30 min before the addition of GFP+ (200 nM) or transferrin (Thermo Fisher Scientific) (50 µg/ml). Cells were further incubated at 37 °C for 4 h before fixation and confocal imaging.

To detect the binding of SARS-CoV-2 to the cell surface, HEK293T-ACE2-GFP cells seeded in 24 well plates that had been coated with fibronectin were treated with 50 µl virus per well at 4 °C for 1 h with centrifugation at 1500 rpm (453 x g) for 60 min. Cells were carefully washed with ice-cold PBS to remove unbound virus and then lysed in a NP40 lysis buffer containing 0.5 % Igepal, 20 mM Tris pH 7.4, 150 mM Sodium Chloride, 2 mM Magnesium Chloride, 0.5 mM EDTA, 1 mM DTT, and a protease inhibitor cocktail. The cell extracts cleared by centrifugation (16,000 x g 5 min) were analyzed by immunoblotting.

qRT-PCR analysis of knockout or knockdown cells

Total RNA was extracted from 3 million HEK293T cells using TriPure reagent (Roche) and purified using RNeasy MinElute Cleanup Kit (Promega) following the standard protocols. The RNA concentration was measured by Nanodrop 2000 UV spectrophotometer, and 1µg total RNA was converted to cDNA using the iScript Reverse Transcription Supermix (BioRad) system. 1µL cDNA was used to perform qPCR using SsoAdvanced SYBR Green supermix kit (BioRad) on a CFX96 machine (BioRad). Data were analyzed using BioRad CFX manager 3.0 software. GADPH was used as a reference gene for the quantification of gene expression levels. Primers used for qRT-PCR were listed in the previous study (*1*). For the RNAseq study, cells were treated independently for 6 h with each drug three times and 6 untreated control samples were included. The treatment conditions are Mitoxantrone 5 µM, Tilorone 10 µM, Raloxifene 10 µM, Piceatannol 10 µM. RNA isolated from control or drug-treated cells (10 µg/sample) were processed by Novagene USA.

Membrane fractionation and heparin Sepharose binding of Mitoxantrone

To fractionate cells, ~15 million cells were treated with 5 µM Mitoxantrone or Banoxantrone for 30 min at 37 °C. Cells were harvested and washed with ice cold PBS. Cells were then resuspended and incubated in 900 µl of a hypotonic buffer (50 mM HEPES, pH 7.3, 25 mM potassium acetate) containing a protease inhibitor cocktail. Cells were homogenized in a Dounce homogenizer with a tight pestle and then subject to differential centrifugation at 1,000 g for 5 min, 7,000 x g for 10min and 100,000 x g for 20 min. The P100 membrane pellet was resuspended in 20 µl NP40 lysis buffer containing 20 mM Tris pH 7.4, 0.5% NP40, 150 mM Sodium Chloride, 2 mM Magnesium Chloride. The absorbance in the cleared membrane extract and the S100 fraction was

measured by a NanoDrop 2000 spectrometer. Note that no absorbance was detected for the S100 fraction even when the samples were measured by a conventional spectrometer with a 10 x light path.

To determine the binding of Mitoxantrone to heparin-coated Sepharose, the compound was diluted to 50 μM in PBS and then incubated with PBS-washed heparin beads or as a control with Sepharose. After brief mixing, the beads were sedimented by centrifugation. The supernatant fractions were analyzed by NanoDrop 2000 for light absorption at the wavelengths specified in the figure legends.

Image processing and statistical analyses

Confocal images were processed using the Zeiss Zen software. To measure fluorescence intensity, we used the Fiji software. Images were converted to individual channels and region of interest was drawn for measurement. Statistical analyses were performed using either Excel or GraphPad Prism 8. Data are presented as mean ± SEM, which was calculated by GraphPad Prism 8. *p*-values were calculated by Student's t-test using Excel. None linear curve fitting and EC_{50} calculation was done with GraphPad Prism8 using the inhibitor response 3 variable model. Images were prepared with Adobe Photoshop and assembled in Adobe Illustrator. All experiments presented were repeated at least twice independently except for the data generated from the Southern Research Institute, which was performed as fee-for-service. The experiments were done once each with two technical repeats. Data processing and reporting are adherent to the community standards.

References

1. Q. Zhang *et al.*, A myosin-7B-dependent endocytosis pathway mediates cellular entry of alpha-synuclein fibrils and polycation-bearing cargos. *Proc Natl Acad Sci U S A* **117**, 10865-10875 (2020).

2. J. K. Millet *et al.*, Production of Pseudotyped Particles to Study Highly Pathogenic Coronaviruses in a Biosafety Level 2 Setting. *J Vis Exp*, (2019).
3. J. K. Millet, G. R. Whittaker, Murine Leukemia Virus (MLV)-based Coronavirus Spike-pseudotyped Particle Production and Infection. *Bio Protoc* **6**, (2016).
4. X. Ou *et al.*, Characterization of spike glycoprotein of SARS-CoV-2 on virus entry and its immune cross-reactivity with SARS-CoV. *Nat Commun* **11**, 1620 (2020).

.

Supplementary Table 1

Reagents and Materials	Source	
Chemicals and viruses		
pHrodo™ Red, succinimidyl ester (pHrodo™ Red, SE)	ThermoFisher Scientific	Cat# P36600
Banoxantrone dihydrochloride	Sigma	Cat# SML1854
Heparin sodium salt from porcine intestinal mucosa	Sigma	Cat# H3393
SARS-CoV-S and SARS-CoV2-S Pseudotyped particles	Codex Biosolutions (Gaithersburg, MD)	Contracted custom production
ATPLite	PerkinElmer	Cat# 6016736
Bright-Glo Luciferase kit	Promega	Cat# E2620
CellTiter-Glo cell viability kit	Promega	Cat# G7572
iScript™ Reverse Transcription Supermix for RT-qPCR	BioRad	Cat# 1708840
SsoAdvanced Universal SYBR Green Supermix	BioRad	Cat# 1725271
Imaging chamber	iBidi	Cat# 80426
TriPure reagent	Sigma	Cat# 11667157001
RNeasy MinElute Cleanup Kit	Qiagen	Cat# 74024
Latrunculin A	TOCRIS	Cat# 3973
NCGC00015693-09	Microsource	01503278
NCGC00015889-11	Microsource	01505622
NCGC00024857-02	BIOMOL	AC-304
NCGC00094226-07	SigmaAldrich	Lopac-P-0453
NCGC00094226-13	Selleck	S3026
NCGC00095196-06	Microsource	02300009
NCGC00164631-05	Sequoia	SRP01785s
NCGC00186034-01	SigmaAldrich	Lopac-K-1015
NCGC00186034-03	SIGMA	K1015
NCGC00249050-02	GVK	FFS-12-73-NCI-3078
Antibodies		
p-Synuclein	Abcam	Cat# ab51253
SARS-CoV-2 S	GeneTex	Cat# GTX632604

Supplementary Figure 1

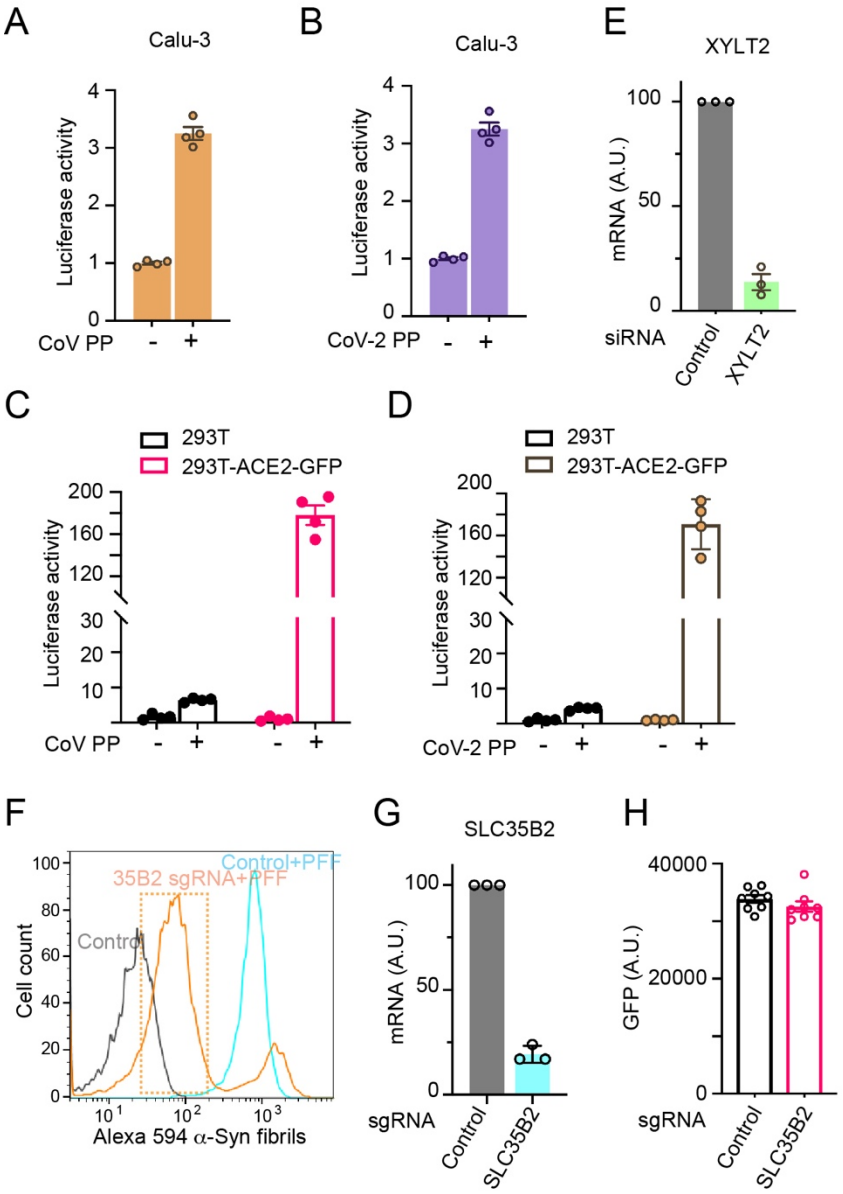

Figure 1 Establishing tools to study ACE2-mediated coronaviral entry.

(**A, B**) The entry of SARS-CoV or SARS-CoV-2 PPs into Calu-3 cells. Uninfected Calu-3 cells or cells infected with the indicated PPs for 48 h were analyzed for luciferase expression. Uninfected cells were normalized to 1. Error bars indicate SEM. N=4.

(**C, D**) The entry of SARS-CoV or SARS-CoV-2 PPs is dependent on ACE2. HEK293T cells or HEK293T-ACE2-GFP cells were either uninfected or infected with the indicated PPs for 24h. The luciferase/GFP ratio was determined to indicate viral entry. Error bars indicate SEM. N=4.

(**E**) Verification of *XYLT2* knockdown by qRT-PCR. A fraction of ACE2-GFP cells transfected with SMARTpooled *XYLT2* siRNAs or a control siRNA for 72 h were analyzed for *XYLT2* expression by qRT-PCR. The remaining cells were used in Figure 1F for viral entry and cell viability assay. Error bars indicate SEM, N=3.

(F) Generating ACE2-GFP cells deficient for *SLC35B2* (*35B2*). ACE2-GFP cells treated with *SLC35B2* sgRNA-expressing lentiviruses were incubated with $Alex^{594}$-labeled (400 nM) α-Syn fibrils for 4h. α-Syn negative *SLC35B2* knockout (KO) cells (dashed box) were identified and collected by FACS.

(**F**) Verification of *SLC35B2* knockdown by qRT-PCR. A fraction of ACE2-GFP cells transfected with SMARTpooled *SLC35B2* siRNAs or a control siRNA for 72 h were analyzed for *SLC35B2* expression by qRT-PCR. The remaining cells were used for viral entry and cell viability assay in Figure 1G. Error bars indicate SEM, N=3.

(**H**) Knockout of *SCL35B2* does not affect ACE2-GFP expression. The ACE2-GFP level in cell extracts used in Figure 1G was determined by a fluorometer.

Supplementary Figure 2

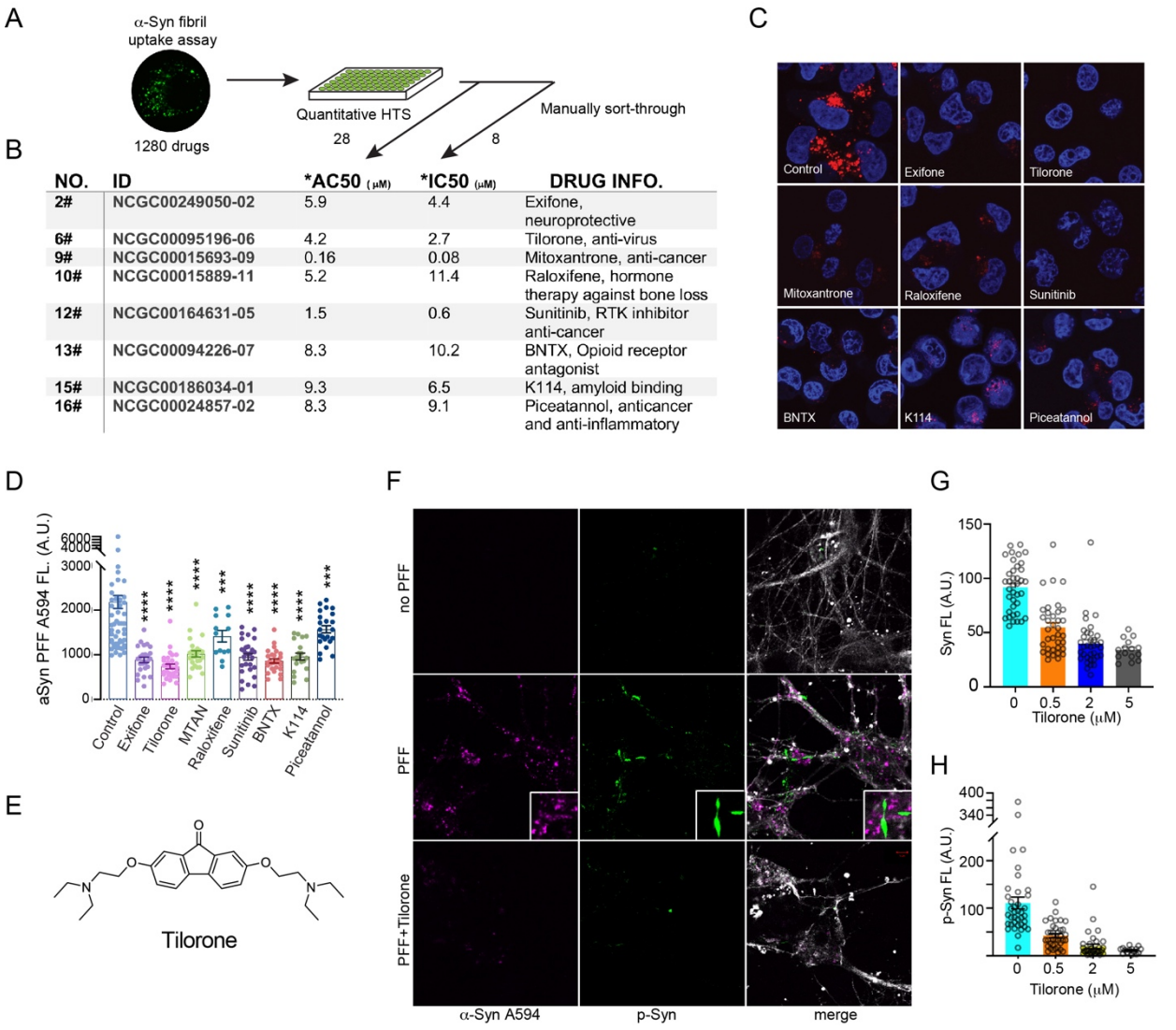

NO.	ID	*AC50 (μM)	*IC50 (μM)	DRUG INFO.
2#	NCGC00249050-02	5.9	4.4	Exifone, neuroprotective
6#	NCGC00095196-06	4.2	2.7	Tilorone, anti-virus
9#	NCGC00015693-09	0.16	0.08	Mitoxantrone, anti-cancer
10#	NCGC00015889-11	5.2	11.4	Raloxifene, hormone therapy against bone loss
12#	NCGC00164631-05	1.5	0.6	Sunitinib, RTK inhibitor anti-cancer
13#	NCGC00094226-07	8.3	10.2	BNTX, Opioid receptor antagonist
15#	NCGC00186034-01	9.3	6.5	K114, amyloid binding
16#	NCGC00024857-02	8.3	9.1	Piceatannol, anticancer and anti-inflammatory

Figure 2 A high-throughput screen identifies inhibitors of HSPG-dependent endocytosis.

(**A**) A scheme of the high-throughput screen (HTS) using fluorescently labeled α-Syn fibrils as a substrate. Each drug was screened at 15 concentrations.

(**B**) A table summary of the eight drugs that inhibit HSPG-dependent uptake ofα-Syn fibrils. AC_{50} was calculated from the automated screen, while IC_{50} was from manually obtained data.

(**C**) Confocal images of HEK293T cells treated with Alexa^{594}-labeled α-Syn fibrils for 3 h in the absence (Control) or presence of the indicated drugs (all at 10 μM except for Mitoxantrone and Sunitinib 5 μM).

(**D**) Inhibition of α-Syn fibril uptake by the identified endocytosis inhibitors in primary neurons. Mouse hippocampal neurons were treated with the indicated compounds at 10 μM or 5 μM for Mitoxantrone and Sunitinib at D.I.V. 7-9 for 30min before incubation with 400 nM A_{594}-labeled α-Syn fibrils for 3 h. Cells were fixed and imaged by confocal microscopy to determine endocytosed α-Syn level in individual cells. Error bars indicate SEM, N=2. ***, $p<0.001$, ****, $p<0.0001$ by unpaired student t-test.

(E) The chemical structure of Tilorone.

(F-H) Tilorone inhibits α-Syn fibril uptake and phosphorylation of endogenous α-Syn in mouse hippocampal neurons. (**F**) Representative confocal images of hippocampal neurons either untreated or treated with Alexa^{594}-labeled preformed α-Syn fibril (PFF) in the absence or presence of 10 μM Tilorone for 14 days. Cells were stained with an antibody against phosphorylated α-Syn (p-Syn) in green. (**G**, **H**) Quantification of the internalized α-Syn fibrils and p-Syn in primary neurons treated with α-Syn together with the indicated concentrations of Tilorone.

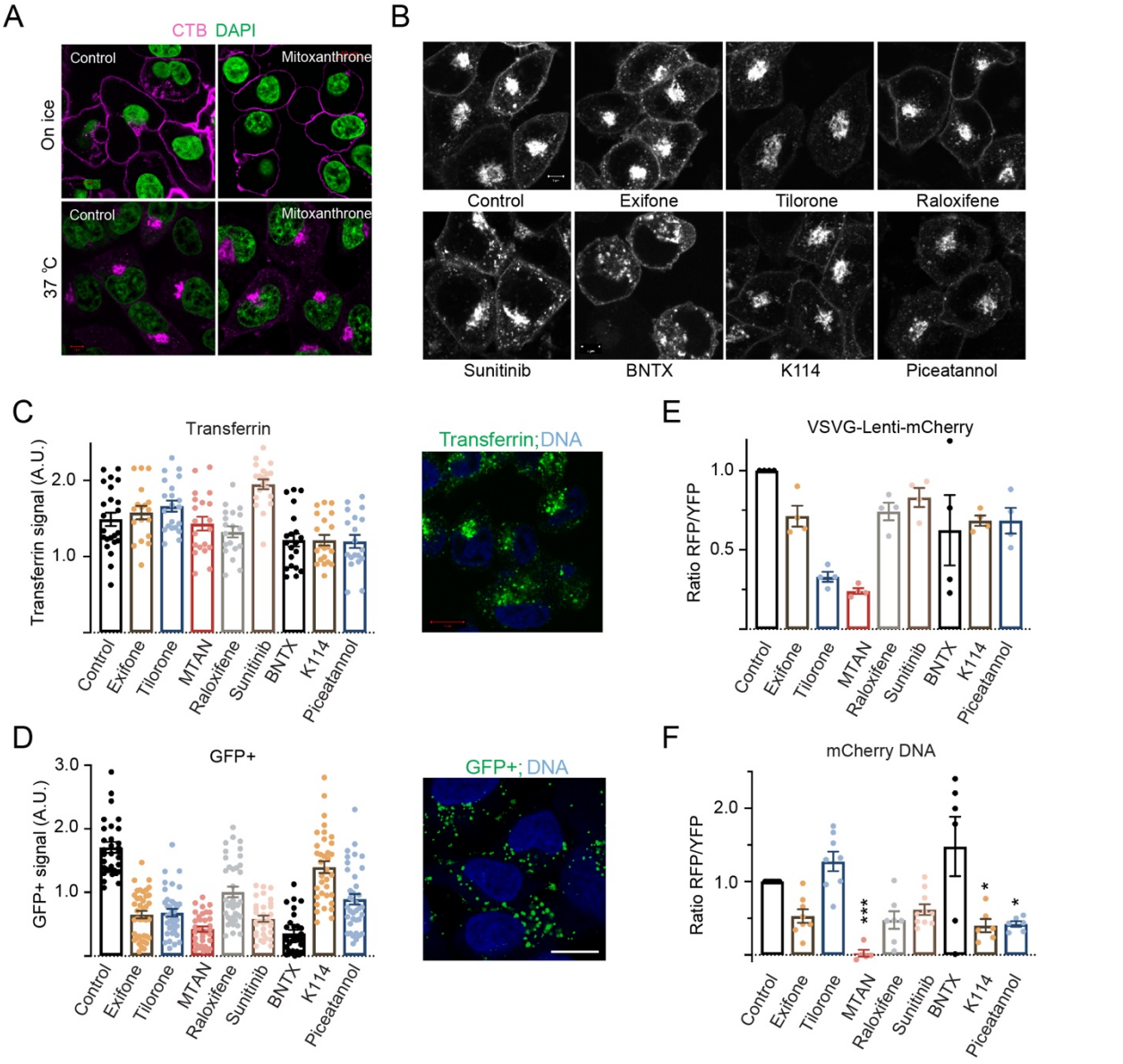

Figure 3 Substrate specificity of the identified drugs.

(A and B) Clatherin-independent endocytosis of cholera toxin B (CTB) chain is not affected by the identified drugs. (A) HEK2923T cells were treated with Mitoxantrone (5 μM) for 1h before incubation with 2 μg/ml Alexa^{555}-labeled CTB on ice for 15min (cell surface binding) or at 37 °C for 20min (uptake). Cells were fixed and stained with DAPI. Note that Mitoxantrone affects neither

the binding of CTB to the cell surface nor its uptake. (B) Cells were treated with the indicated drugs at 10 μM (Sunitinib at 5 μM) for 1h before incubation with CTB at 37 °C for 20 min.

(**C**) The effect of drugs on the endocytosis of Transferrin. HEK293T cells were pretreated with the compounds for 30 min before incubation with Alexa^{488}-labeled Transferrin (50 μg/ml) at 37 °C for 4 h. Cells were fixed, stained with DAPI (blue), and imaged by confocal microscopy. The image shows an example of Transferrin uptake in control cells. The graph shows the quantification of internalized Transferrin signal in individual cells. A.U., arbitrary unit. Error bars indicate SEM.

(**D**) The effect of drugs on the endocytosis of GFP+. HEK293T cells treated with the indicated compounds for 30 min were incubated with 100 nM GFP+ for 4 h before heparin wash, fixation, and staining with Hoechst (Blue). The graph shows internalized GFP+ signals in individual cells. The image shows an example of GFP+ uptake in control cells. A.U. arbitrary units. Error bars indicate SEM. N=2.

(**E**) The effect of drugs on the entry of VSVG-pseudotyped lentivirus bearing a mCherry reporter. HEK293T cells stably expressing YFP were treated with the inhibitors as in C, infected with VSVG-Lenti-mCherry in the presence of the inhibitors for 6 h. Cells were then incubator in virus free, inhibitor free medium for 48 h before quantification of the mCherry /YFP ratio by a fluorometer. Error bars indicate SEM. N=4.

(F) The effect of drugs on the entry of plasmid DNA bearing a mCherry reporter. As in E, except that cells were transfected with a mCherry-bearing plasmid. Error bars indicate SEM. N=dot number. *, $p<0.05$, *** $p<0.001$ by unpaired student t-test.

Supplementary Figure 4

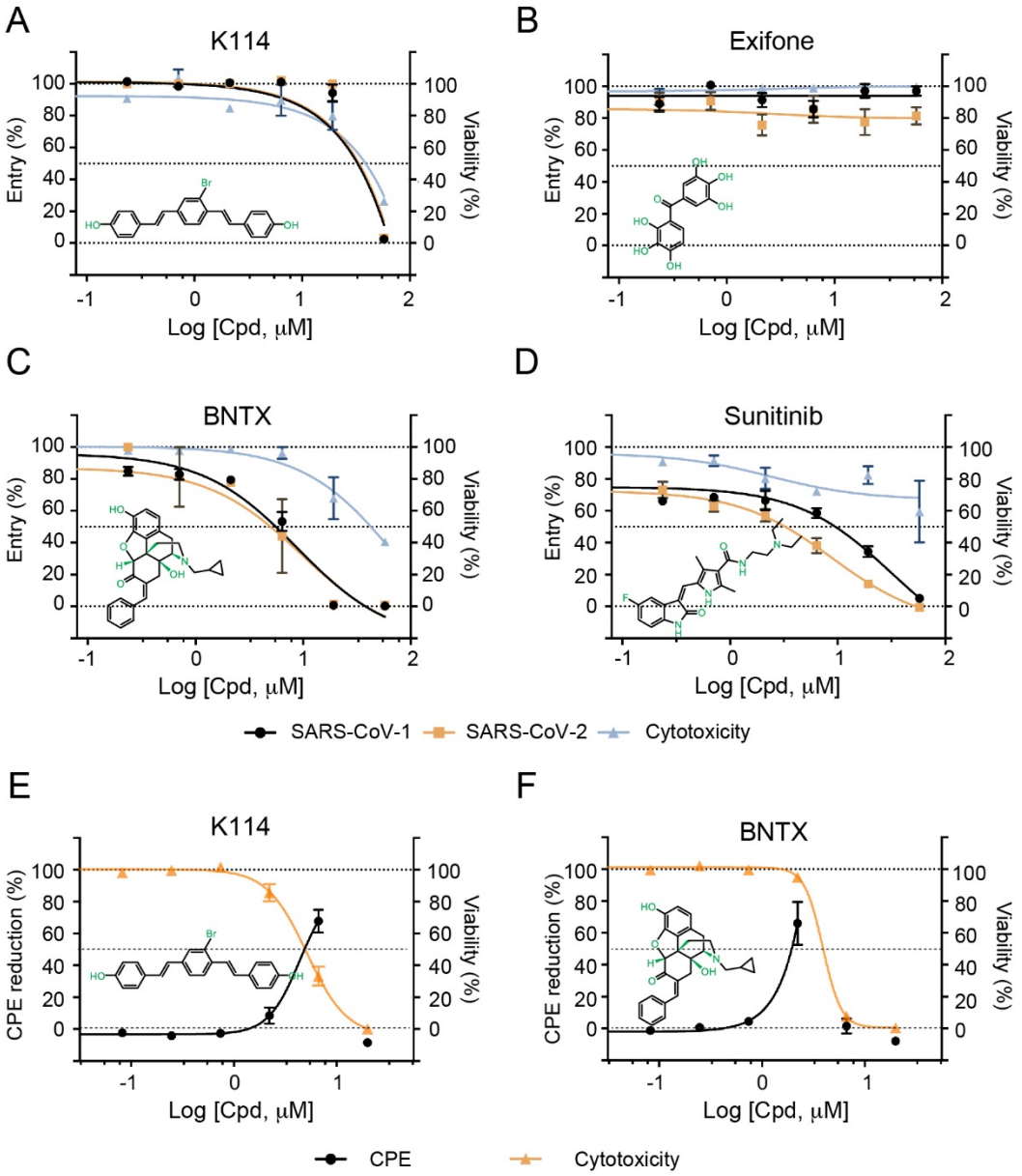

Figure 4 The effect of endocytosis inhibitors on coronavirus entry.

(A-D) HEK293 cells stably expressing ACE2-GFP were infected with SARS-CoV or SARS-CoV-2 PPs in the presence of the indicated drugs. % of viral entry was determined by luciferase level. Cells treated with the inhibitors without the virus were used to determine drug toxicity. Error bars indicate SEM, N=4.

(**E** and **F**) The effect of the indicated drugs on the cytopathic phenotype induced by wildtype SARS-CoV-2. Vero E6 cells were treated with the indicated drugs in the presence of SARS-CoV-2 (black curves) or in the absence of the virus (orange curves) and then assayed for cell viability. (CPE, Cytopathic effect). Error bars indicate SEM, N=2.

Supplementary Figure 5

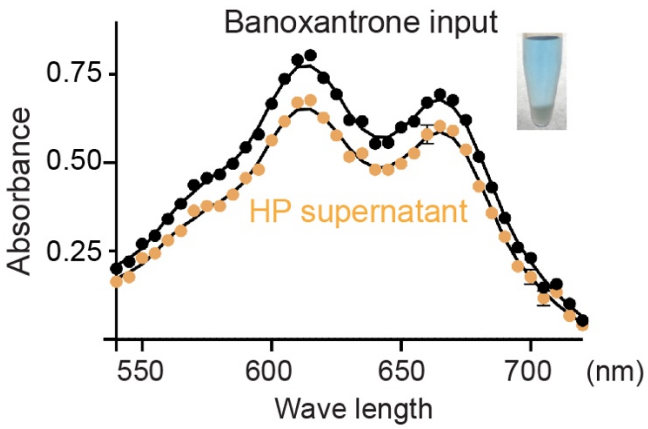

Figure 5 Banoxantrone does not bind heparin beads.

Banoxantrone (50 μM) was incubated with heparin (HP)-coated Sepharose for 5 min. The picture shows the sample after centrifugation. The absorbance spectra of the HP-bead-depleted supernatant were measured together with a fraction of the input.

Supplementary Figure 6

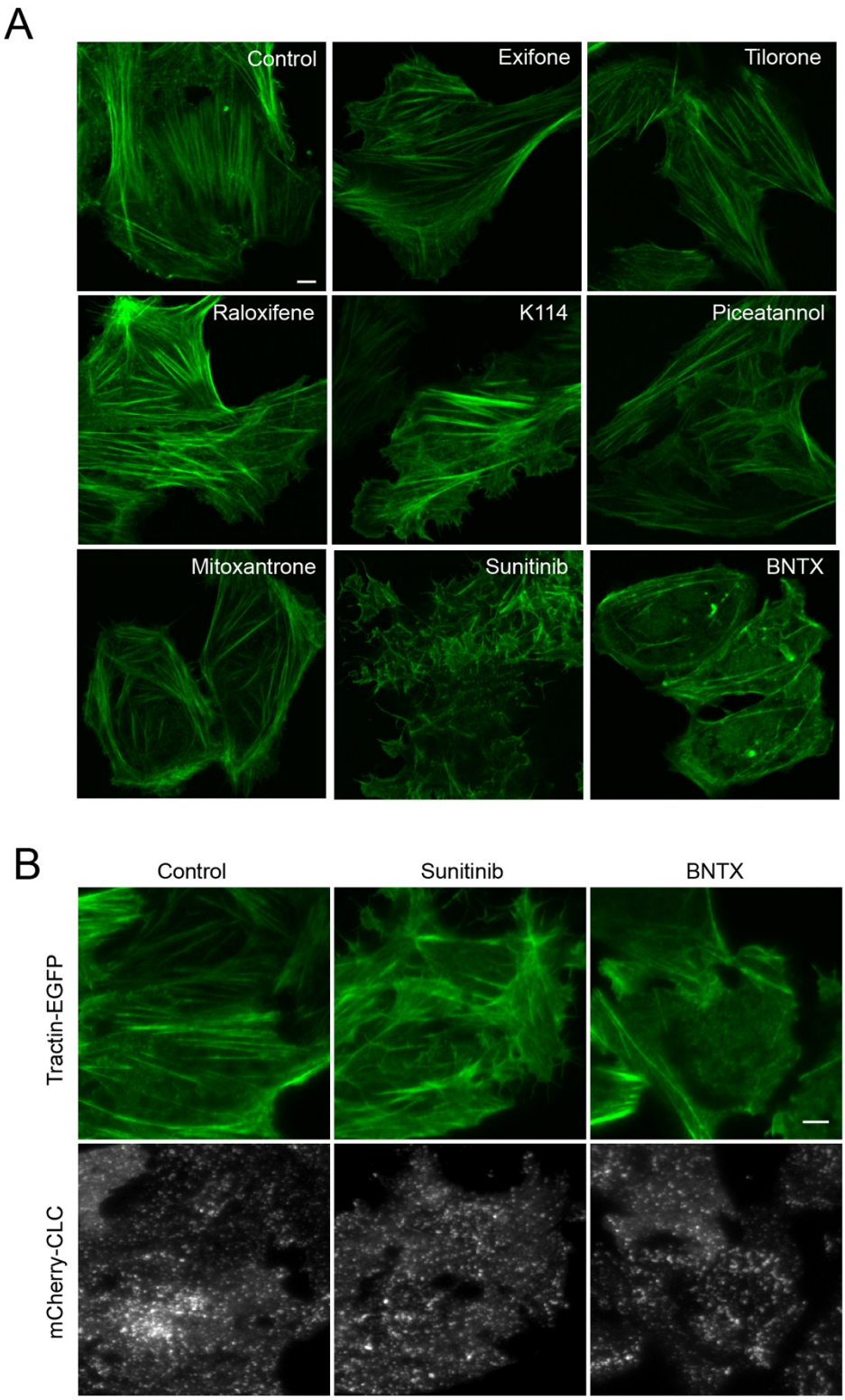

Figure 6 The effect of endocytosis inhibitors on the actin cytoskeleton network.

(**A**) Confocal images of U2OS cells stably expressing Tractin-EGFP, which have been treated with the indicated inhibitors at 10 μM (Mitoxantrone and Sunitinib 5μM) for 1h. Scale bar, 5 μm.

(**B**) TIRF images of drug-treated U2OS cells stably expressing Tractin-EGFP and mCherry-Clathrin light chain (CLC). CLC was used to focus on the plasma membrane. Scale bar, 5μm.

Supplementary Figure 7

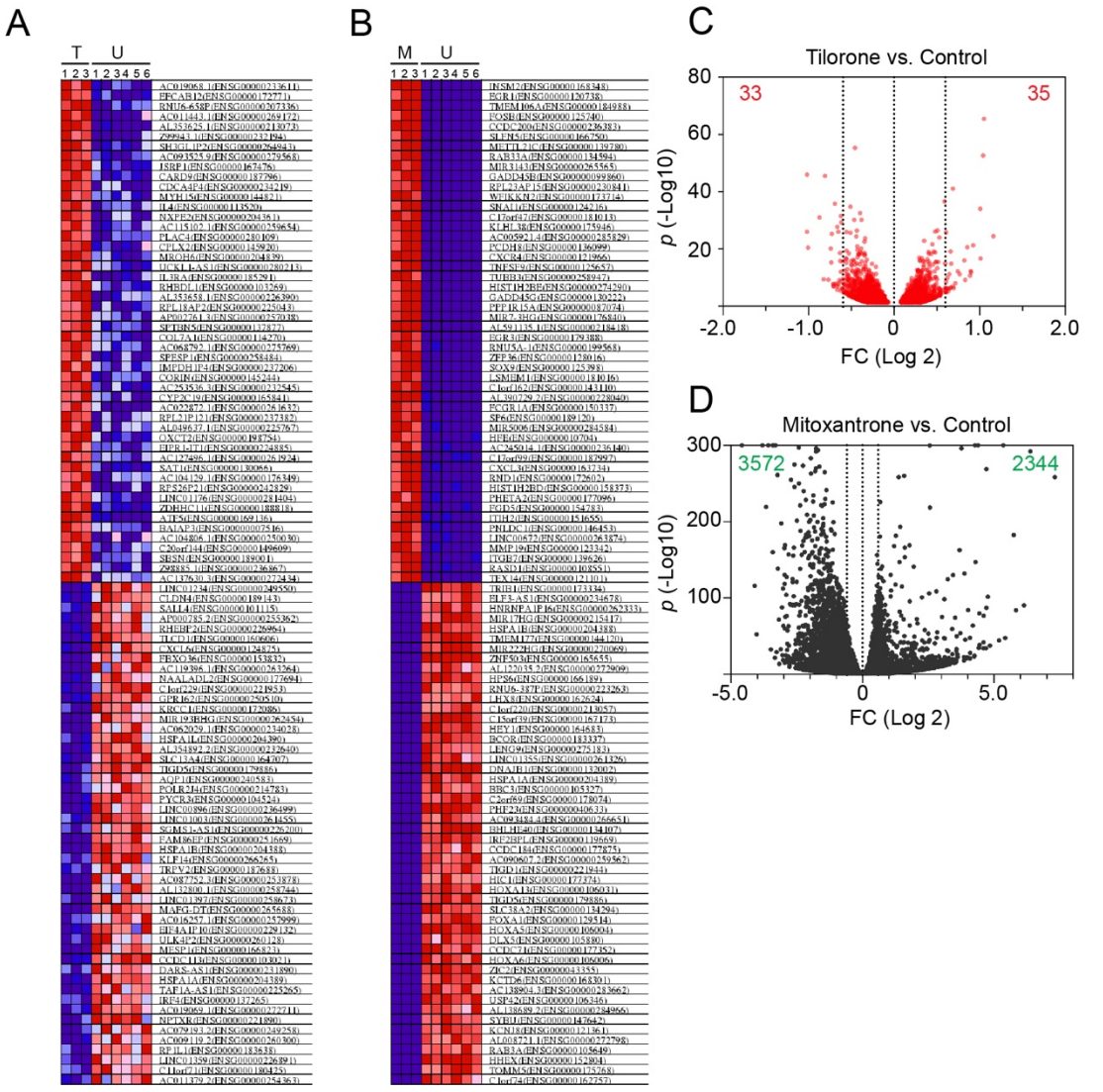

Figure 7 Gene expression analysis of Tilorone- and Mitoxantrone-treated cells.

(**A**) A heat map summary of the most induced or down-regulated genes by Tilorone (10 μM 6 h) in HEK293T cells.

(**B**) A heat map summary of the most induced or down-regulated genes by Mitoxantrone (5 μM 6 h) in HEK293T cells.

(**C**) A volcano plot shows the genes affected by Tilorone. Note that both the number of genes (shown by the number) and the scale of the expression changes in Tilorone-treated cells are small.

(**D**) A volcano plot shows the genes affected by Mitoxantrone.

Supplementary movies

Movie 1

A U2OS cell expressing Tractin-EGFP.

Movie 2

The cell shown in movie 1 was imaged after treatment with Sunitinib 5 μM for 15 min. Note the increased assembly of actin filaments causes new filopodia formation on the cell surface.

Movie 3

A Tractin-EGFP-expressing U2OS cell was imaged after treatment with Sunitinib 5 μM for 60 min.

Movie 4

The same Tractin-EGFP-expressing U2OS cell in movie 3 was imaged at a different confocal plan where the stress fibers are located.

Movie 5

A U2OS cell expressing Tractin-EGFP.

Movie 6

The cell shown in movie 5 was imaged after treatment with BNTX 10 μM for 5min.